Scripta Materialia 152 (2018) 117–121

Contents lists available at ScienceDirect

Scripta Materialia

journal homepage: www.elsevier.com/locate/scriptamat

Regular article

Influence of ZrO_2 alloying effect on the thermophysical properties of fluorite-type Eu_3TaO_7 ceramics

Lin Chen, Peng Song *, Jing Feng *

Faculty of Material Science and Engineering, Kunming University of Science and Technology, Kunming 650093, People's Republic of China

ARTICLE INFO

Article history:
Received 20 December 2017
Received in revised form 28 March 2018
Accepted 30 March 2018
Available online xxxx

Keywords:
TBCs
Rare earth tantalates
Thermal conductivity
Thermal expansion
Phase stability

ABSTRACT

ZrO_2 alloying effect is applied in fluorite-type Eu_3TaO_7 ceramics to decrease thermal conductivity and improve thermal expansion performance. The thermal conduction mechanism of Eu_3TaO_7 ceramics can be adjusted by ZrO_2 alloying effect and the lowest thermal conductivity reaches 1.37 $W \cdot m^{-1} \cdot K^{-1}$ at 900 °C. The Young's modulus of x mol% ZrO_2-Eu_3TaO_7 ceramics decreases with the increasing ZrO_2 content, as ZrO_2 alloying effect can weaken the bonding strength of Eu_3TaO_7 and then increase the thermal expansion coefficients (10.7×10^{-6} K^{-1}, 1200 °C). Due to the excellent thermophysical properties, ZrO_2-Eu_3TaO_7 ceramics exhibit great potentiality as high-temperature thermal insulation materials.

The development of current gas turbine engine has been the result of continual improvement in a wide variety of engineering techniques including turbine design, combustion and materials [1–3]. In order to design the higher gas efficiency engines, the operation temperature of gas turbine engine must be increased. To achieve this goal, thermal barrier coatings (TBCs) are one of the most important materials in gas turbine engine. The primary function of TBCs is to provide a low thermal conductivity barrier to heat transfer from the hot gas to the surface of alloy components in the engine [4–6]. The base requirements of TBCs include low thermal conductivity, low elastic modulus, high thermal expansion coefficients and so on [1,3,5]. Nowadays, besides the problems arise in substrate, the problems in TBCs are obvious too. The most popular TBC materials are yttria-stabilized zirconia (YSZ) ceramics, whose operation temperature is below 1200 °C, because of the phase transition [7,8]. It is difficult for YSZ to meet the demand of gas turbine engine and many researchers seek for new kinds of TBCs to replace YSZ.

Over the past several decades years, a class of ceramics are identified as materials with low thermal conductivity, i.e., rare-earth zirconate $RE_2Zr_2O_7$ (RE = rare earth elements) ceramics [7,9,10]. Because of the unique crystal structure: pyrochlore or fluorite, the high concentration of oxygen vacancy (12.5%) of $RE_2Zr_2O_7$ leads to the low thermal conductivity [11]. The oxygen vacancy can scatter phonon strongly by the missing atoms and missing interatomic linkages, which seriously decrease the phonon mean free path [12–14]. Besides, the thermal conductivity of $RE_2Zr_2O_7$ ceramics can be reduced by various methods. Ti^{4+} is used to substitute Zr^{4+} in $Gd_2Zr_2O_7$ ceramics to reduce thermal conductivity [15]; Yb^{3+} is applied to substitute La^{3+} in $La_2Zr_2O_7$ ceramics to obtain the glass-like thermal conductivity [10]. To research new materials applied as TBCs, C. G. Levi and D. R. Clarke propose that rare earth tantalates may be promising TBC materials [16,17]. The thermophysical properties of rare earth tantalates $RETaO_4$ and $RETa_3O_9$ ceramics are reported in literatures [18–20] by J. Feng et al. Based on the ternary diagram of ZrO_2-$TaO_{2.5}$-$YO_{1.5}$, the thermal conductivity of Y_3TaO_7 ceramics is relatively low (2.4–1.5 $W \cdot m^{-1} \cdot K^{-1}$, 100–1000 °C) [17]. From this point of view, RE_3TaO_7 ceramics may exhibit low thermal conductivity, attributed to the similar crystal structure as $RE_2Zr_2O_7$ ceramics. However, only the crystal structure and magnetic properties of RE_3TaO_7 ceramics have been reported [21,22]. In our unpublished paper the research of RE_3TaO_7 (RE = La, Nd, Sm, Eu, Gd, Dy) ceramics shows that RE_3TaO_7 (RE = La, Nd) ceramics exhibit obvious thermal radiation effect, which will increase thermal conductivity evidently at high temperature (≥600 °C). Phase transition has been detected in Sm_3TaO_7 ceramics at 940 °C and RE_3TaO_7 (RE = Eu, Gd, Dy) ceramics exhibit the same crystal structure that results in the similar thermal conductivity and thermal expansion coefficients. Furthermore, Eu_3TaO_7 ceramics possess less density than RE_3TaO_7 (RE = Gd, Dy) ceramics, indicating that Eu_3TaO_7 ceramics demand less cohesive force than RE_3TaO_7 (RE = Gd, Dy) ceramics when they are sprayed as coatings.

In this work, we focused on the thermophysical properties of Eu_3TaO_7 ceramics and ZrO_2 alloying effect was applied to optimize the thermophysical properties. The properties including elastic modulus, thermal expansion coefficients, phase stability and thermal conductivity of x mol% ZrO_2-Eu_3TaO_7 (x = 0, 3, 6, 9, 12, 15) ceramics were

* Corresponding authors.
E-mail address: vdmzsfj@sina.com. (J. Feng).

https://doi.org/10.1016/j.scriptamat.2018.03.042
1359-6462/

investigated. We highlighted the x mol% ZrO_2-Eu_3TaO_7 ceramics as promising TBCs due to the outstanding thermophysical properties. The supplementary materials offered the information about materials preparation, phase structure characterization and properties measurement.

The phase structure of x mol% ZrO_2-Eu_3TaO_7 ceramics is characterized via X-ray diffraction (XRD) and Raman spectra. Fig. 1(a) shows that the XRD patterns of Eu_3TaO_7 ceramics are consistent with the PDF#38-1413 and no secondary phase is detected, indicating that Eu_3TaO_7 ceramics crystallize in order orthorhombic phase with Cmcm space group. Fig. 1(b) shows that each sample exhibits the similar XRD patterns and no secondary phase is detected. The XRD peaks between 12° to 22° of 2-Theta are shown in Fig. 1(c) as they are too weak to be revealed in Fig. 1(b) and they are consistent with the PDF#38-1413. The intensity of XRD peaks (201) and (111) in Fig. 1(c) decreases with the increasing ZrO_2 content, which is caused by the change of grain orientation of Eu_3TaO_7 ceramics. Based on literature [19], RE_3TaO_7 (RE = Ho-Lu) ceramics exhibit the disorder cubic phase, as the ionic radius of Ho-Lu is shorter than La-Dy. The similar phenomenon may occur in x mol% ZrO_2-Eu_3TaO_7 ceramics as the ionic radius of Zr^{4+} (0.084 nm) is shorter than Eu^{3+} (0.107 nm). Fig. 1(d) and (f) show the normalized Raman peaks of x mol% ZrO_2-Eu_3TaO_7 ceramics under 532 and 785 nm wavelengths. One can see that at least six characteristic Raman peaks are observed in each sample and they are analogous. Fig. 1(d) and (f) show that the Raman peak V_1 disappears attributed to the increasing ZrO_2 content, which can be observed more obviously in Fig. 1(e). In addition, Fig. 1(e) shows that the intensity of the main Raman peak decreases with the increasing ZrO_2 content. Generally, the Raman peak V_2 derives from the collinear Ta—O—Ta bond in TaO_6 octahedron and it points to one of the most specific features of RE_3TaO_7 ceramics with orthorhombic phase [23]. Evidently, the characteristic stretching motion of Ta—O—Ta band V_2 shifts to higher wavenumber with the increasing ZrO_2 content. According to Ref [24], the V_2 peak of RE_3TaO_7 ceramics with order orthorhombic phase will shift to higher wavenumber due to the decreasing RE^{3+} ionic radius. Herein, it is believed that Zr^{4+} ions have substituted Eu^{3+} cations to decrease the RE^{3+} ionic radius of x mol% ZrO_2-Eu_3TaO_7 ceramics. The disappearance of V_1 peak is because that V_1 peak shifts to higher wavenumber and its intensity decreases with the increasing ZrO_2 content. Furthermore, the Raman peaks between 100 and 300 cm^{-1} root in the RE—O bonds [25], and the number of these peaks decreases with the increasing ZrO_2 content, indicating the reduction of RE—O bond characteristic. Based on Fig. 1(d) and (f), no obvious difference of Raman peak is detected among Eu_3TaO_7 ceramics with different ZrO_2 content, indicating that each x mol% ZrO_2-Eu_3TaO_7 ceramics crystallize in the same order orthorhombic phase with Cmcm space group.

The microstructures of x mol% ZrO_2-Eu_3TaO_7 ceramics are observed under the backscattered electron model (BSE) except Eu_3TaO_7 ceramics, which is observed under the secondary electron model (SE) as shown in Fig. 2. Fig. 2(b)–(f) show that all grains exhibit the similar atomic number contrast. Combined with the results of XRD and Raman, it is believed that no secondary phase exists in these x mol% ZrO_2-Eu_3TaO_7 ceramics. Besides, the grain boundaries are obvious, the grain size is about 1–10 μm and only little pores are detected. The surface EDS scanning of 12 mol% ZrO_2-Eu_3TaO_7 ceramics is shown in Fig. 2(g)–(k). We can see that no obvious agglomeration of any element is detected in this sample as it takes the advantage of solid-state reaction.

Table 1 list that the Young's modulus of x mol% ZrO_2-Eu_3TaO_7 ceramics decreases with the increasing ZrO_2 content and the similar trend can be observed in the Bulk and Shear modulus. In general, Young's modulus increases with the increasing bonding strength, thus, the bonding strength of Eu_3TaO_7 ceramics decreases with the increasing ZrO_2 content; besides, the decreasing modulus can be expected because of the structural relaxation. As the crystal structure integrity of Eu_3TaO_7 relies on the Ta-O octahedrons [15], the decreasing bonding strength

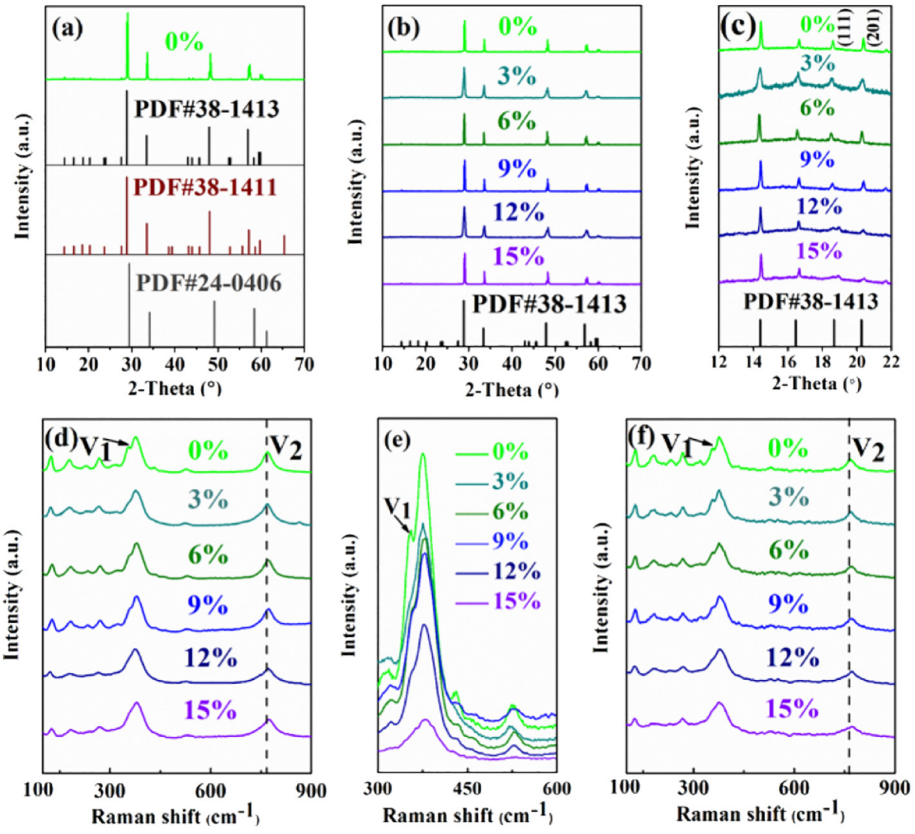

Fig. 1. Phase characterization of x mol% ZrO_2-Eu_3TaO_7 (x = 0, 3, 6, 9, 12, 15) ceramics; (a) XRD patterns of Eu_3TaO_7 compared with standard PDF cards; (b) XRD patterns of each sample, 10° ≤ 2-Theta ≤ 70°; (c) XRD of each sample, 12° ≤ 2-Theta ≤ 22°; (d) normalized Raman spectrum under 532 nm; (e) the main Raman peak under 532 nm; (f) normalized Raman spectrum under 785 nm.